



Evaluation of MR elastography for prediction of lymph node metastasis in prostate cancer

Bing Hu¹ · Ying Deng¹ · Jingbiao Chen¹ · Sichi Kuang¹ · Wenjie Tang¹ · Bingjun He¹ · Linqi Zhang¹ · Yuanqiang Xiao¹ · Jun Chen² · Phillip Rossman² · Arvin Arani² · Ziyang Yin² · Kevin J. Glaser² · Meng Yin² · Sudhakar K. Venkatesh² · Richard L. Ehman² · Jin Wang¹

Received: 12 October 2020 / Revised: 17 January 2021 / Accepted: 9 February 2021 / Published online: 2 March 2021
© The Author(s), under exclusive licence to Springer Science+Business Media, LLC part of Springer Nature 2021

Abstract

Purpose To assess the relationship between MRE stiffness of prostate cancer (PCa) and the extent of lymph node metastasis (LNM) in patients with PCa undergoing radical prostatectomy (RP) and extended pelvic lymph node dissection (ePLND).

Materials The local institutional review board approved this retrospective study. We retrospectively analyzed 49 patients, who had undergone MRE, mpMRI and pelvic MRI on a 3.0 T MRI scanner, with histopathological confirmed PCa after RP (from June 2015 to December 2019). For each patient, preoperative clinical data and characteristics of MRE, mpMRI and pelvic MRI were recorded. Independent-samples t test, univariate and multivariate logistic regression analyses were performed. And receiver operating characteristic (ROC) analysis were performed to compare the diagnostic performances of multivariate models with the Briganti 2019 nomogram.

Results PCa MRE stiffness and maximum diameter were independent predictors of LNM. When PCa MRE stiffness at 60 Hz (odds ratio [OR] = 20.223, $P = 0.013$) and maximum diameter (OR = 4.575, $P = 0.046$) were combined, the sensitivity and specificity were 100% and 91.9% to predict LNM. When PCa MRE stiffness at 90 Hz (OR = 7.920, $P = 0.013$) and maximum diameter (OR = 2.810, $P = 0.045$) were combined, the sensitivity and specificity were 100% and 86.5% to predict LNM. The areas under curves (AUCs) of the combinations were higher than the AUC of the Briganti 2019 nomogram (0.982 vs. 0.904, $P = 0.040$ [60 Hz]; 0.975 vs. 0.904, $P = 0.060$ [90 Hz], respectively).

Conclusions MRE-based assessment of PCa stiffness may be useful for predicting LNM of PCa preoperatively and noninvasively.

Keywords Lymph node metastasis · Magnetic resonance elastography · Multiparametric magnetic resonance imaging · Prostate cancer

Abbreviations

MRE	MR elastography
mpMRI	Multi-parametric MRI
PCa	Prostate cancer
LNM	Lymph node metastasis
RP	Radical prostatectomy
ePLND	Extended pelvic lymph node dissection
ECM	Extracellular matrix

Introduction

Prostate cancer (PCa) is one of the most common cancers in men and the global burden of this disease is rising [1]. Lymph node metastasis (LNM) is an essential prognostic factor in patients with PCa, which has shown to be a valuable predictor for biochemical recurrence-free survival, metastatic-free survival, and overall survival in PCa [2]. Extended pelvic lymph node dissection (ePLND) is the established method of staging regional nodes. However, this invasive technique may not have any direct benefit on cancer outcomes [3]. It may result in more substantial adverse consequences in terms of operating time, blood loss, length of stay, and postoperative complications [3]. Therefore, a noninvasive imaging method is needed to reduce or eliminate the need for ePLND.

✉ Jin Wang
Wangjin3@mail.sysu.edu.cn

¹ Department of Radiology, Third Affiliated Hospital, Sun Yat-Sen University (SYSU), No 600, Tianhe Road, Guangzhou, Guangdong 510630, People's Republic of China

² Department of Radiology, Mayo Clinic, 200 First Street SW, Rochester, MN 55905, USA

Many noninvasive imaging techniques have been used to preoperatively characterize the LNM of PCa. Conventional CT and MRI rely on size criteria to determine lymph node status [4], and one meta-analysis found that the pooled sensitivity and specificity for CT were 42% and 82%, for MRI were 39% and 82%, respectively [5]. Von Below et al. [6] indicated that multiparametric MRI (mpMRI) of the prostate enables tumor and LNM detection, and DWI has a sensitivity and specificity of 55% and 90% in detecting LNM of PCa. However, a major drawback of DWI is the potential for susceptibility artifacts to cause both signal loss and image distortion [7]. Novel imaging techniques such as MR lymphography with superparamagnetic iron oxide (SPIO) nanoparticles and targeted positron emission tomography imaging (PET) are currently under development and appear to improve lymph node staging of PCa [10]. Winter et al. [8] published a detection rate of 90% with a 100% sensitivity for LNM using SPIO nanoparticles as magnetic tracer. In the study on the role of PET to detect LNM of PCa, Chang et al. [9] found that the sensitivity and specificity were 75% and 100%. However, these novel imaging techniques remains in research field with no clinical routine application.

Due to an increase in cellular density, microvascularization and the destruction of the glandular architecture, PCa is stiffer than normal prostate tissue [11]. With digital rectal examination (DRE), a physician can assess the stiffness of the prostate gland qualitatively and detect PCa from benign tissue, however, manual palpation is a subjective evaluation and dependent on the physician's skill and experience. Moreover, this method does not allow the physician to palpate the entire prostate manually. Recently, elastography including ultrasound elastography and MR elastography have been developed to noninvasively assess the mechanical properties of tissues [12]. Ultrasound-based elastography has been shown to be useful in the diagnosis of PCa [13, 14]. However, this technique is based on two-dimensional elastography and is dependent on operator experience [15].

MR elastography (MRE) can directly visualize three-dimensional propagating mechanical shear waves and quantitatively measure tissue mechanical properties in biological tissues [16]. It is sensitive to the mechanical response of pathophysiologic changes in soft tissue [17]. The most established clinical application of MRE in the abdomen is detecting hepatic fibrosis [18]. Increasing experience and ongoing research are leading to the exploration of its application in other abdominal organs, such as the spleen [19], kidney [20], pancreas [21], and prostate [22–24].

Previous evidences have shown that MRE has potential for detecting, localizing, and staging prostate cancer. Sahebjavaher et al. [25] indicated that MRE was more accurate than DWI in detecting histopathology-proven malignancy in ex-vivo. Li et al. [26] found that the MRE-assessed mean elasticity was significantly higher in the lesions with PCa

than in regions with prostatitis and normal peripheral zone. Dittmann et al. [27] demonstrated the feasibility of in vivo multifrequency MRE of the prostate, and indicated that MRE stiffness maps displayed many details of potential interest for cancer diagnosis. However, the diagnostic value of MRE of the prostate for LNM has not been investigated before.

The purpose of this study was to assess the diagnostic performance of MRE by measuring the mechanical properties of the primary PCa, identifying PCa LNM preoperatively in patients who underwent radical prostatectomy (RP) and ePLND.

Materials and methods

Patients

From June 2015 to December 2019 the local institutional review board approved the use of a database of 455 patients who had undergone MRE, mpMRI and pelvic MRI for retrospective review. We excluded 406 patients as followed: technical failure of MRE ($n=9$); having had locoregional therapy before MRI/MRE examinations ($n=48$); no treatment was performed ($n=216$); non-RP treatments ($n=91$); without ePLND in patients underwent RP ($n=37$); maximum diameter of the lesion less than 1 cm ($n=5$). Finally, 49 patients (mean age, 68.39 years; range, 53–83 years) were enrolled in this study. They were categorized into two groups based on the histopathological results of ePLND. Twelve patients with regional LNM were included in group 1: PCa with LNM (positive LNM), and 37 patients without regional LNM were included in group 2: PCa without LNM (negative LNM) (Fig. s1).

For each patient, the following clinical and pathologic parameters were collected: age, height, weight, body mass index (BMI), serum prostate serum antigen (PSA), PSA density (PSA/prostate volume), the time between MRI/MRE and biopsy, the time between MRI/MRE and surgery, biopsy Gleason grade groups, and RP Gleason grade groups. The diagnoses of PCa and LNM were determined by the histopathologic results.

MRI protocol

MRI was performed on a 3.0 T scanner (GE, Discovery MR750, Milwaukee, WI) with 8-channel phased-array torso coils (GE, Milwaukee, WI).

MRE was performed with a custom-built passive driver, developed by Mayo Clinic (Rochester, MN). The passive driver was composed of a cylindrical drum with a 10-cm-diameter, 0.5-mm-thick, polycarbonate diaphragm with a 5-mm-deep cavity and a 5-mm solid acrylic backing

(Supplementary Fig. 1). It was applied to the lower abdominal wall, partially overlapping the symphysis pubis. Continuous acoustic vibrations at 60 Hz and 90 Hz, which were generated by an active driver (Resoundant Inc., Rochester, MN) and transmitted to the passive driver via a flexible vinyl tube, were used to produce propagating shear waves in the prostate, respectively. A test vibration was first applied to allow the patient to get familiar with the vibration.

A free-breathing, multislice, EPI, 3D-MRE sequence was used to image the waves. Clinical mpMRI and pelvic MRI were also acquired. Pulse sequences and parameters of MRE, mpMRI, and pelvic MRI were summarized in Table 1.

MRE analysis

The MRE acquired displacement fields were processed using a 3D direct inversion (DI) algorithm [28–30] of the Helmholtz wave equation after applying the curl operator,

to calculate stiffness maps within the entire field-of-view of MRE sequence. The shear stiffness was calculated from the wave images using by first calculating the curl and the divergence of the wave information, and then using the curl information to perform a direct inversion of the Helmholtz wave equation to calculate the complex-valued shear modulus which was used to derive the MRE parameters. The processing steps were applied automatically to generate quantitative images of tissue shear stiffness maps, in units of kiloPascals (kPa).

Image registration was used with a software (RadiAnt DICOM Viewer, Version 2020.2, Medixant, Poznan, Poland). Mean stiffness of PCa was calculated and recorded in kPa using a manually specified region of interest (ROI). The ROIs were drawn independently by two radiologists (B.H. and J.W.), who were experienced in reading liver and prostate MRE images (> 1000 studies read in the past 3 years), blinded to all clinical and

Fig. 1 Flowchart of patient population in current study. *MRE* MR elastography, *PCa* prostate cancer, *RP* radical prostatectomy, *ePLND* extended pelvic lymph node dissection, *LNM* lymph node metastasis

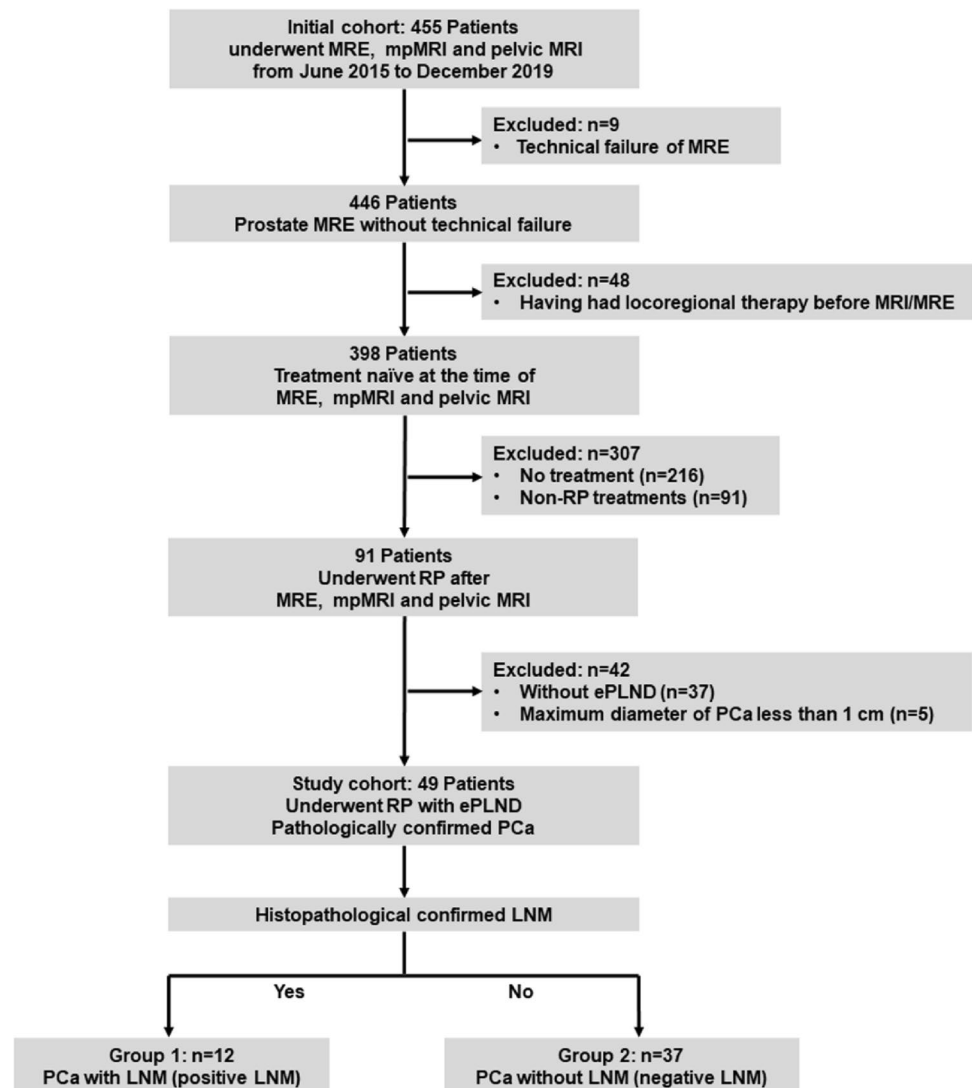


Table 1 Pulse sequences and parameters of MRE, mpMRI and pelvic MRI

Parameter	Pulse sequence	TR (ms)	TE (ms)	Slice thickness (mm)	Interslice gap (mm)	Number of slices	FOV (mm)	Matrix	Resolution (mm)	NEX	Acquisition time (m:s)
MRE											
60 Hz	SE-EPI	1334	52	3	0	20	240×240	80×80	3×3	1	2:00
90 Hz	SE-EPI	1334	52	3	0	20	240×240	80×80	3×3	1	2:00
mpMRI											
Ax T2WI	FSE	3611	80	3	0	20	160×160	320×224	0.5×0.7	4	3:22
Ax fs-T2WI	FSE	3485	110	3	0	20	160×160	320×224	0.5×0.7	4	3:22
Ax T1WI	FSE	723	24.3	3	1	30	320×320	320×224	1×1.4	1	1:16
High <i>b</i> -value DWI	EPI	3545	89.7	3	0	30	220×220	128×128	1.7×1.7	10	1:53
Multiple <i>b</i> -values DWI	EPI	3896	90	3	0	30	220×220	128×128	1.7×1.7	1–6	3:43
DEC	LAVA	4.4	1.3	3	0	24	340×272	320×200	1×1.4	1	2:16
Pelvic MRI											
Sag T2WI	FSE	3514	110	4	1	20	240×240	320×224	0.8×1.1	2	2:00
Cor T2WI	FSE	3795	110	4	1	20	240×240	320×224	0.8×1.1	2	2:09
Sag T1WI+C	LAVA	4.5	1.4	3	1.5	48	280×224	280×256	1×0.9	2	0:40
Cor T1WI+C	LAVA	4.2	1.3	4	2	40	360×360	320×224	1.1×1.6	2	0:40
Ax T1WI+C	LAVA	4.8	1.4	5	2.5	56	320×256	320×192	1×1.3	2	0:39

The high *b*-value was $b = 1500 \text{ s/mm}^2$. Multiple *b*-values DWI included $b = 0, 30, 50, 80, 100, 150, 200, 400, 600$ and 800 sec/mm^2 , and the NEX were 2, 1, 1, 1, 2, 4 and 6, respectively. For ADC map calculation, ten *b*-values ($0\text{--}800 \text{ s/mm}^2$) were used. Dynamic contrast-enhanced (DCE) images were obtained before, during, and after gadopentetate dimeglumine administration (0.1 mmol/kg , 2 mL/sec). Each sequence was performed at an 8-s interval

MRE MR elastography, SE-EPI spin echo based echo planer imaging, FSE fast spin echo, LAVA liver acceleration volume acquisition, Cor coronal, Sag sagittal, Ax axial, fs fat saturate, DWI diffusion weighted imaging, DEC dynamic contrast-enhanced, ADC apparent diffusion coefficient, TR repetition time, TE echo time, FOV field of view, NEX number of excitation

histopathological results. And these two radiologists were also experienced in mpMRI and pelvic MRI (with 16 and 27 years for B.H. and J.W., respectively, > 3000 studies read in the past 3 years). The ROIs were drawn on the T2WI (PCa in transition zone) and DWI (PCa in peripheral zone) covering as much tumor as possible while excluding tumor edges (where partial-volume effects likely affected the calculated stiffness), areas of significant wave interference, and any other artifacts, then the ROIs were copied to 3D elastogram, ADC and other MRI sequences.

MpMRI and pelvic MRI analysis

All mpMRI and pelvic MRI Images were independently reviewed by the same two radiologists (B.H. and J.W.) who reviewed MRE images. All images and lesions were scored and reported according to the Prostate Imaging Reporting and Data System (PI-RADS) version 2.1 criteria [31]. For each patient, the following radiological variables were recorded: prostate volume, PCa location, PI-RADS score, maximum diameter of PCa, PCa volume, PCa invasiveness, PCa ADC, presence of enlarged LNs and presence of LNs with restricted diffusion. The maximum diameters of three dimensions of PCa lesions were measured and PCa volume was calculated using ellipsoid formulation [31]: (max anteroposterior diameter) × (max transverse diameter) × (max longitudinal diameter) × 0.52. For ADC calculation, ROIs were manually drawn on the ADC map including only the inner aspect of the lesion to reduce partial volume effects. Information regarding PCa invasiveness, such as extraprostatic extension and seminal vesicles invasion, was recorded. For the definition of enlarged LNs on T2WI, a threshold of 10 mm in the short-axis for oval nodes and 8 mm for round nodes was used [10]. LN with restricted diffusion was defined hyperintense on high-*b*-value DWI ($b = 1500 \text{ s/mm}^2$). The two reviewers met to make final decisions by consensus for discordant cases.

Nomogram evaluation

Following the instruction of the Briganti 2019 nomogram [32], the points of serum PSA, extracapsular extension and/or seminal vesicle invasion, biopsy Gleason grade group, maximum diameter of PCa and percentage of cores at biopsy were summed to get the total score for each patient. Then the risk of LNM of each patient was recorded. A 7% cut-off was used to calculate the sensitivity, specificity, positive predictive value (PPV), negative predictive value (NPV), and accuracy for the prediction of LNM.

Histopathological evaluation

All patients with PCa had both 12-core systematic biopsy and whole-mount radical prostatectomy specimens produced. Lesion locations and Gleason grades on whole-mount specimens were annotated by a genitourinary pathologist with 15 years' experience, who was blinded to MRI results.

LNs (encompassing obturator, internal iliac, external iliac, common iliac and nodes) were handled by the same genitourinary pathologist. Whether there were LNMs or not were recorded.

Statistical analysis

To compare variables between two groups, categorical variables were analyzed using Chi square test, and continuous data were evaluated using independent-samples *t* test or Mann–Whitney *U* test.

Interobserver agreement of the PCa stiffness measurements between two radiologists was evaluated using the intraclass correlation coefficient (ICC) along with its 95% CI. The level of agreement was defined as follows: 0.00–0.20, poor; 0.21–0.40, fair; 0.41–0.60, moderate; 0.61–0.80, good; and 0.81–1.0, excellent.

Univariate and multivariate logistic regression analyses were performed to test the association between the preoperative variables and LNM. Because there was collinearity between PCa MRE stiffness at 60 Hz and at 90 Hz, two multivariable models were fitted, respectively. As a measure of the relationship between the variables and the outcomes, the β coefficient, standard error (SE) and odds ratios (OR) were reported. Nomograms were constructed on the basis of the prediction models. The sensitivity, specificity, PPV, NPV, and accuracy of each significant imaging finding and combinations of findings for predicting LNM were also calculated.

Receiver operating characteristic (ROC) analysis of multivariate models and the Briganti 2019 nomogram for predicting LNM was performed. The areas under the curves (AUCs) of them were calculated and compared.

Statistical softwares (SPSS version 25, SPSS, Chicago, IL, USA; and R version 3.6.1, R Foundation for Statistical Computing, Vienna, Austria) were used for statistical analyses (J.C.). The significance level was indicated by a *P* value less than 0.05.

Results

Baseline characteristics

Baseline demographic characteristics of patients and pathologic characteristics of PCa with LNM are demonstrated in Table 2. Baseline variables including age, height, weight,

Table 2 Demographic and pathologic data of the study cohort

Parameter	Overall (<i>n</i> = 49)	PCa with LNM (<i>n</i> = 12)	PCa without LNM (<i>n</i> = 37)	<i>P</i> value
Age (year)				0.446
Mean ± SD	68.39 ± 6.83	67.08 ± 6.61	68.81 ± 6.93	
95% CI	66.43–70.35	62.88–71.28	66.50–71.12	
Height (m)				0.810
Mean ± SD	1.66 ± 0.05	1.66 ± 0.03	1.66 ± 0.06	
95% CI	1.64–1.67	1.64–1.68	1.64–1.68	
Weight (kg)				0.933
Mean ± SD	62.63 ± 8.36	62.83 ± 9.79	62.57 ± 7.99	
95% CI	60.23–65.03	56.61–69.05	59.90–65.23	
BMI (kg/m ²)				0.982
Mean ± SD	22.75 ± 2.67	22.74 ± 3.11	22.76 ± 2.56	
95% CI	21.99–23.52	20.76–24.71	21.90–23.61	
Serum PSA (ng/ml)				0.010
Mean ± SD	27.79 ± 34.08	62.76 ± 51.67	16.45 ± 13.90	
95% CI	18.00–37.58	29.93–95.59	11.82–21.09	
PSA density (ng/ml/ml)				0.006
Mean (median)	0.65 (0.40)	1.15 (1.16)	0.48 (0.37)	
IQR	0.22–0.82	0.40–1.62	0.19–0.61	
Time between MRI/MRE and biopsy (d)				0.832
Mean (median)	4(3)	5(4)	4(3)	
IQR	1–6	1–7	1–6	
Time between MRI/MRE and surgery (d)				0.880
Mean (median)	15 (13)	16 (14)	15 (13)	
IQR	7–20	7–27	7–20	
Biopsy Gleason grade groups (%)				0.001
1	13 (26.5)	1 (8.3)	12 (32.4)	
2	10 (20.4)	0 (0)	10 (27.0)	
3	9 (18.4)	2 (16.7)	7 (18.9)	
4	10 (20.4)	5 (41.7)	5 (13.5)	
5	7 (14.3)	4 (33.3)	3 (8.1)	
RP Gleason grade groups (%)				0.006
1	8 (16.3)	0 (0)	8 (21.6)	
2	13 (26.5)	1 (8.3)	12 (32.4)	
3	8 (16.3)	2 (16.7)	6 (16.2)	
4	10 (20.4)	5 (41.7)	5 (13.5)	
5	10 (20.4)	4 (33.3)	6 (16.2)	

PCa prostate cancer, LNM lymph node metastasis, SD standard deviation, CI confidence interval, BMI body mass index, PSA prostate specific antigen, IQR interquartile, RP radical prostatectomy, Percentages are referred to the total of patient of the correspondent population

BMI, the time between MRI/MRE and biopsy, and the time between MRI/MRE and surgery were similar in both groups ($P > 0.05$).

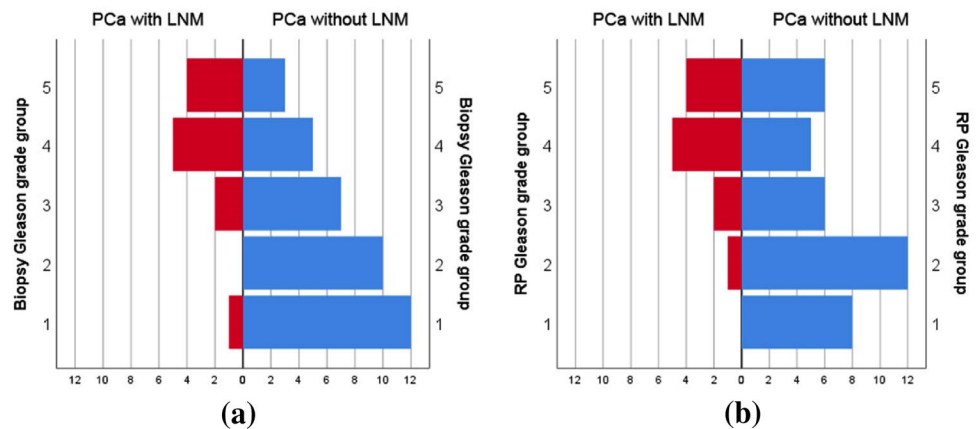
With regard to histologic features, the distributions of biopsy and RP Gleason grade groups were significantly different between two groups ($P = 0.001$ and $P = 0.006$, respectively). Both biopsy and RP Gleason grade group 4 or more were more frequently observed in group 1 than group 2 (75.0% vs. 21.6%, and 75.0% vs. 29.7%, respectively).

(Fig. 2). Moreover, both serum PSA ($P = 0.010$) and PSA density ($P = 0.006$) in group 1 were significantly higher than those in group 2.

MRI characteristics

The radiological characteristics of the study cohort were summarized in Table 3. The sizes of ROIs were 4.51 ± 3.80 (95% CI 2.85–6.18) cm². The PCa stiffnesses were measured

Fig. 2 The distributions of biopsy Gleason grade groups were significantly different between PCa with LNM group and PCa without LNM group ($P=0.001$) (a). And the distributions of RP Gleason grade groups were also significantly different between two groups ($P=0.006$) (b)



on 3D elastogram (Fig. 3). There were excellent interobserver reproducibilities of PCa stiffness at 60 Hz and 90 Hz, with an ICC of 0.839 (95% CI 0.731–0.906) and 0.887 (95% CI 0.809–0.935), respectively (Supplementary Fig. 4). The mean PCa stiffness in group 1 was significantly higher than that in group 2 both at 60 Hz (5.22 ± 0.81 kPa vs. 3.24 ± 0.93 kPa, $P < 0.001$) and at 90 Hz (7.11 ± 1.08 kPa vs. 4.71 ± 1.13 kPa, $P < 0.001$), respectively (Fig. 4). There is a moderate correlation between RP Gleason grade group and MRE stiffness at 60 Hz ($r=0.414$, $P=0.003$). And there is a moderate correlation between RP Gleason grade group and MRE stiffness at 90 Hz ($r=0.585$, $P < 0.001$).

In univariate analyses, clinical variables (including serum PSA, PSA density, biopsy Gleason grade groups and RP Gleason grade groups) and radiological variables (including PCa MRE stiffness at 60 Hz and 90 Hz, maximum diameter of PCa, ADC, PCa invasiveness, LN with restricted diffusion) were significantly associated with LNM ($P < 0.05$). In multivariate analysis, because there was collinearity between PCa MRE stiffness at 60 Hz and at 90 Hz, two multivariable models were fitted, respectively. In model 1, PCa MRE stiffness at 60 Hz (OR = 20.223, $P=0.013$) and maximum diameter (OR = 4.575, $P=0.046$) were independent significant variables for predicting LNM of PCa. In model 2, PCa MRE stiffness at 90 Hz (OR = 7.920, $P=0.013$) and maximum diameter (OR = 2.810, $P=0.045$) were independent significant predictors. There was no significant difference ($P=0.468$) for ROC between PCa MRE stiffness at 60 Hz (AUC of 0.937) and maximum diameter of PCa ≥ 2.0 cm (AUC of 0.892). And there was no significant difference ($P=0.325$) for ROC between PCa MRE stiffness at 90 Hz (AUC of 0.946) and maximum diameter of PCa ≥ 2.0 cm (AUC of 0.892). Univariate and multivariate logistic regression analyses for predicting lymph node metastasis of PCa were reported in Table 4. Regression coefficient-based nomograms were constructed from these significant variables (Fig. 5).

The sensitivity, specificity, PPV, NPV, and accuracy of the combination in model 1 were 100%, 91.9%, 80.0%, 100%, and 93.9%, respectively, with an AUC value of 0.982. The sensitivity, specificity, PPV, NPV, and accuracy of the combination in model 2 were 100%, 86.5%, 70.6%, 100%, and 89.8%, respectively, with an AUC value of 0.975. Diagnostic performances of all the variables were reported in Table 5 and Supplementary Table 1. ROC curves of model 1 combination and model 2 combination for predicting LNM were demonstrated in Fig. 6. There was no statistically significant difference between the AUCs of model 1 and model 2 (0.982 vs. 0.975, $P=0.383$).

Risk of LNM relied on Briganti nomogram

Following the instruction of the Briganti 2019 nomogram [32], the risk of LNM of each patient was calculated. There was significant difference in the risk of LNM between group 1 (median = 87.5%, IQR = 63.2–90.0%) and group 2 (median = 10.0%, IQR = 3.5–37.0%), ($P < 0.001$). Using a 7% cut-off, the sensitivity, specificity, PPV, NPV and accuracy were 100%, 40.5%, 35.3%, 100% and 55.1%, respectively.

The ROC curve of the probability of predicted value calculated by the Briganti 2019 nomogram for predicting LNM were demonstrated in Fig. 6. The AUC of model 1 combination was significantly higher than the AUC of the Briganti 2019 nomogram (0.982 vs. 0.904, $P=0.040$). The AUC of model 2 combination was higher than the AUC of the Briganti 2019 nomogram, while there was no statistically significant (0.975 vs. 0.904, $P=0.060$).

Discussion

Our results demonstrated that PCa MRE stiffness and maximum diameter were independent and significant predictors of LNM of PCa. Combining these two MRI findings for predicting LNM resulted in high predictive accuracy, with

Table 3 Radiological characteristics of the study cohort

Variable	Overall (n=49)	PCa with LNM (n=12)	PCa without LNM (n=37)	P value
MRE				
PCa stiffness at 60 Hz (kPa)				<0.001
Mean ±SD	3.73 ± 1.24	5.22 ± 0.81	3.24 ± 0.93	
95% CI	3.37–4.08	4.70–5.73	2.93–3.55	
PCa stiffness at 90 Hz (kPa)				<0.001
Mean ±SD	5.30 ± 1.52	7.11 ± 1.08	4.71 ± 1.13	
95% CI	4.86–5.73	6.42–7.80	4.33–5.09	
mpMRI				
Prostate volume (cm ³)				0.236
Mean (median)	46.48 (35.19)	57.31 (45.97)	42.97 (30.62)	
IQR	25.60–58.21	32.70–57.05	24.67–60.31	
PCa Location (%)				0.552
PZ	29 (59.2)	7 (58.3)	22 (59.5)	
TZ	12 (24.5)	1 (8.3)	11 (29.7)	
PZ + TZ	8 (16.3)	4 (33.3)	4 (10.8)	
PI-RADS score				0.004
4	17 (34.7)	0 (0)	17 (45.9)	
5	32 (65.3)	12 (100.0)	20 (54.1)	
Maximum diameter of PCa (cm)				<0.001
Mean (median)	2.33 (1.80)	3.93 (3.65)	1.82 (1.60)	
IQR	1.30–3.00	2.55–4.35	1.05–2.15	
PCa volume (cm ³)				<0.001
Mean (median)	9.89 (2.04)	29.70 (18.10)	3.47 (1.20)	
IQR	0.56–7.34	5.26–30.74	0.45–3.45	
PCa ADC (10 ⁻³ mm ² /s)				0.003
Mean ±SD	0.62 ± 0.13	0.55 ± 0.08	0.65 ± 0.13	
95% CI	0.59–0.66	0.50–0.60	0.60–0.69	
PCa invasiveness (%)				0.001
Absent	25 (51.0)	1 (8.3)	24 (64.9)	
Present	24 (49.0)	11 (91.7)	13 (35.1)	
LN with restricted diffusion (%)				0.014
Absent	19 (38.8)	1 (8.3)	18 (48.6)	
Present	30 (61.2)	11 (91.7)	19 (51.4)	
Pelvic MRI				
Enlarged LN (%)				<0.001
Absent	43 (87.8)	6 (50.0)	37 (100)	
Present	6 (12.2)	6 (50.0)	0 (0)	

PCa prostate cancer, LNM lymph node metastasis, MRE MR elastography, SD standard deviation, CI confidence interval, PZ peripheral zone, TZ transition zone, IQR interquartile, ADC apparent diffusion coefficient, LN lymph node. Percentages are referred to the total of patient of the correspondent population

high sensitivity, specificity, and accuracy. In addition, we presented the nomograms for individualized risk estimation that calculates the numeric probability of LNM. MR elastography has promising potential in predicting lymph node metastasis of prostate cancer.

MRE can generate shear waves, create an image of the propagation of these waves in tissue, and assess the stiff properties of tissue quantitatively. MRE technique of prostate, which are similar to the steps for liver MRE, has the

following steps. First, a passive driver is placed on the body wall and is activated with acoustic pressure waves that are conducted through a plastic tube that is connected to the wave actuator to deliver shear waves to the tissue. Second, the MRE acquisition is a modified phase-contrast sequence. Special motion encoding gradients are used to sensitize the sequence to the cyclic tissue motion that is caused by the shear waves. Third, the wave images were processed to calculate corresponding elastograms.

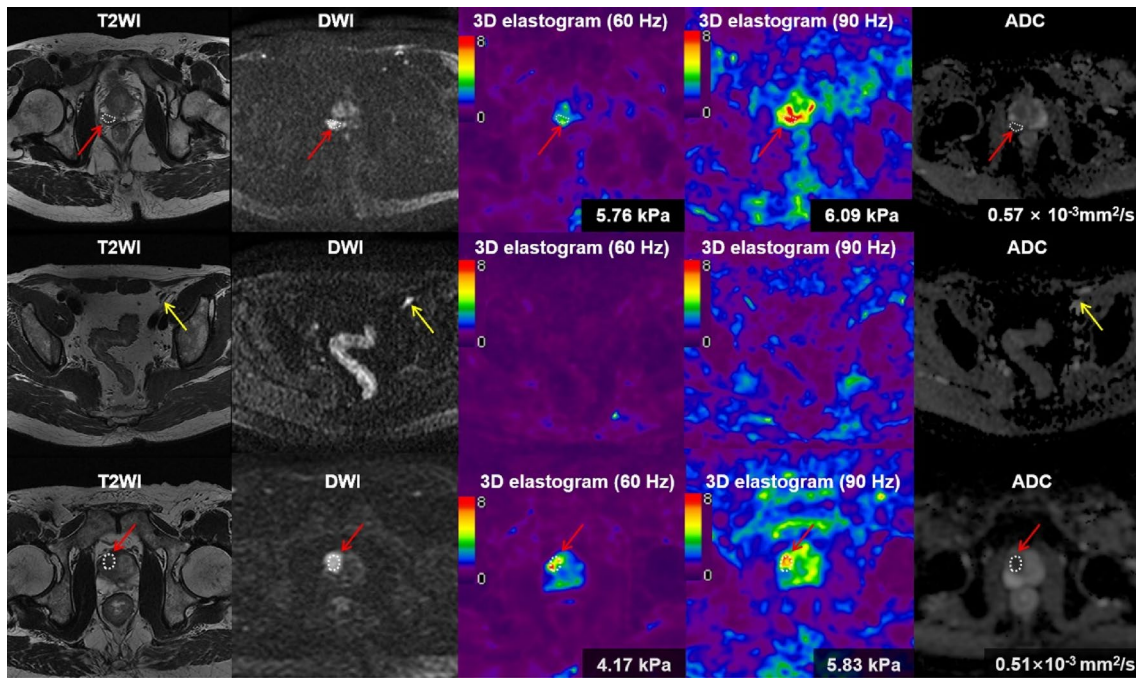


Fig. 3 First row, from left to right (a–e); second row, from left to right (f–j); third row, from left to right (k–o). A 60-year-old male man with prostate cancer (a–e) and with lymph node metastasis (f–j). The tumor (red arrow) was shown moderate hypointense on T2 weighted image (T2WI) (a), and hyperintense on diffusion-weighted image (DWI) (b). The tumor stiffness was 5.76 kPa on 3D elastogram at 60 Hz (c) and was 6.09 kPa at 90 Hz (d), respectively. The apparent diffusion coefficient (ADC) value of the tumor was $0.57 \times 10^{-3} \text{mm}^2/\text{s}$ (e). An enlarged lymph node (yellow arrow)

was found on T2WI (f) and DWI (g). Because the stiffness value of LN was similar with the stiffness value of surrounding structures, the LN was hardly visible in the elastogram (h, i). 73-year-old man with prostate cancer (red arrow) without lymph node metastasis (k–o). The tumor was shown homogenous moderate hypointense on T2WI (k), and hyperintense on DWI (l). The tumor stiffness was 4.17 kPa on 3D elastogram at 60 Hz (m) and was 5.83 kPa at 90 Hz (n). The ADC value of the tumor was $0.51 \times 10^{-3} \text{mm}^2/\text{s}$ (o)

Fig. 4 The mean PCa stiffness at 60 Hz in the positive LNM group (5.22 ± 0.81 kPa) was significantly higher than that in the negative LNM group (3.24 ± 0.93 kPa, $P < 0.001$) (a). And the mean PCa stiffness at 90 Hz in positive LNM group (7.11 ± 1.08 kPa) was significantly higher than that in negative LNM group (4.71 ± 1.13 kPa, $P < 0.001$) (b)

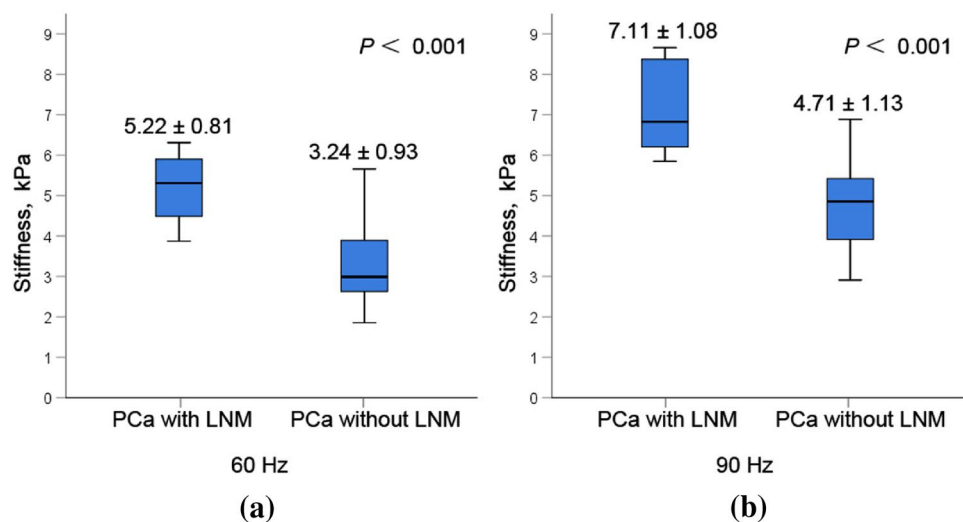


Table 4 Univariate and multivariate logistic regression analysis for predicting lymph node metastasis of prostate cancer

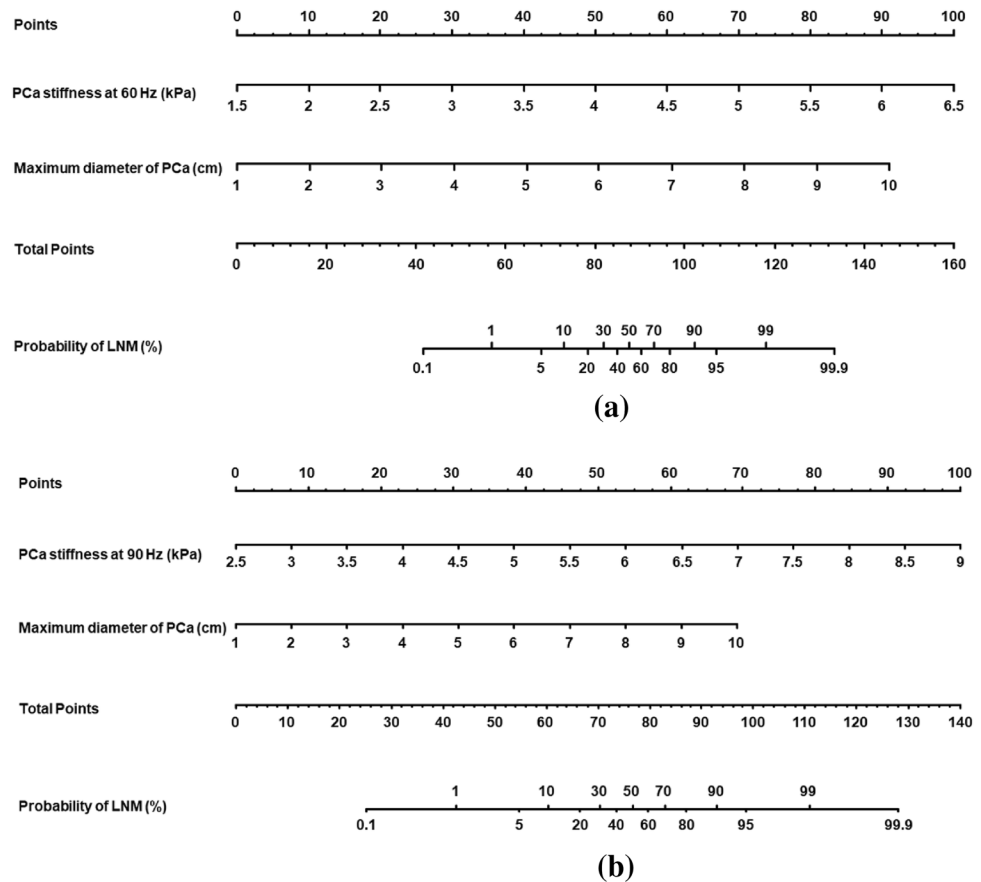
Variable	Univariate analysis				Multivariate analysis*			
	β	SE	OR	<i>P</i>	β	SE	OR	<i>P</i>
Serum PSA	0.056	0.020	1.058	0.004				
Biopsy Gleason grade groups	0.932	0.320	2.539	0.004				
PCa stiffness at 60 Hz	2.167	0.642	8.732	0.001	3.007	1.215	20.223	0.013
PCa stiffness at 90 Hz	2.219	0.740	9.201	0.003	2.069	0.833	7.920	0.013
Maximum diameter of PCa	1.271	0.388	3.566	0.001	1.521 (1.033**)	0.762 (0.515)	4.575 (2.810)	0.046 (0.045)
ADC	-7.413	3.383	0.001	0.028				
PCa invasiveness	3.011	1.100	20.308	0.006				
LN with restricted diffusion	2.344	1.095	10.421	0.032				

SE standard error, OR odds ratio, PSA prostate specific antigen, RP radical prostatectomy, PCa prostate cancer, MRE MR elastography, ADC apparent diffusion coefficient, LN lymph node

*Because there was collinearity between PCa MRE stiffness at 60 Hz and at 90 Hz, two multivariable models were fitted, respectively, according to forward stepwise regression based on maximum likelihood estimation. In model 1, PCa MRE stiffness at 60 Hz and maximum diameter were independent significant variables for predicting LNM of PCa. In model 2, PCa MRE stiffness at 90 Hz and maximum diameter were independent significant predictors

**The numbers in parentheses indicated that the corresponding values in model 2

Fig. 5 Nomograms of multivariate analysis model 1 (a) and model 2 (b) to predict the probability of LNM in a patient with PCa. Predictor points are found on uppermost point scale that corresponds to each variable. On the bottom scale, points for all variables are added and translated into probability of LNM



In our study, the range of MRE stiffness values of PCa either with LNM or without LNM were similar to those reported earlier [26, 33, 34], which demonstrated that MRE

was sensitive to changes in the stiffness of tissue. Asbach et al. [33] performed multifrequency MRE at 60, 70 and 80 Hz, that provided quantitative maps of tissue mechanical

Table 5 Diagnostic performance of two significant imaging findings and their combination for predicting lymph node metastasis of prostate cancer

Variable	AUC	Sens %	Spec %	PPV %	NPV %	Accu %
Model 1						
PCa MRE stiffness at 60 Hz ≥ 4.14 kPa	0.937	91.7	83.8	64.7	96.9	85.7
Maximum diameter of PCa ≥ 2.0 cm	0.892	91.7	73.0	52.4	96.4	77.6
Combination	0.982	100	91.9	80.0	100	93.9
Model 2						
PCa MRE stiffness at 90 Hz ≥ 5.79 kPa	0.946	100	83.8	66.7	100	87.8
Maximum diameter of PCa ≥ 2.0 cm	0.892	91.7	73.0	52.4	96.4	77.6
Combination	0.975	100	86.5	70.6	100	89.8

AUC area under the receiver operating curve, Sens sensitivity, Spec specificity, PPV positive predictive value, NPV negative predictive value, Accu accuracy, PCa prostate cancer, MRE MR elastography

parameters of the prostate. They found that PCa was characterized by stiff tissue properties and reduced water diffusion. Reiter et al. [34] examined fourteen fresh prostate specimens from men with clinically significant PCa by MRE at 500 Hz immediately after radical prostatectomy in a 9.4 T scanner. They found that the difference of storage modulus was significant ($P < 0.001$) between healthy segments (5.44 ± 4.40 kPa) and cancerous segments (10.84 ± 4.65 kPa). They suggested that prostate MRE had the potential to improve diagnostic performance of mpMRI.

The color bar at the image of 3D elastogram from purple to red indicated the stiffness value from low to high. The stiffness value of surrounding structures was lower than that of prostate and PCa. So, most of surrounding structures were in purple and blue (Fig. 3). While the colors of prostate and PCa were yellow and red. Because the stiffness value of LN

was similar with the stiffness value of surrounding structures, the LN was hardly visible in the elastogram.

Our study also showed that PCa MRE stiffness was a significant marker for predicting LNM, with high odds ratio and high predictor point on the nomograms. According to the previous studies, an increased extracellular matrix (ECM) stiffness may contribute to an overall increase in tumor stiffness [35], and some components of ECM are involved in the process of lymph node metastasis [36]. A hypothesis might be that increased MRE stiffness of PCa could predict LNM by reflecting the remodeling of ECM. In our study, we used a pelvic wall flexible soft passive driver, developed by Mayo Clinic, to do prostate MRE examinations. We supposed that it was more comfortable and less invasive than endorectal MRE, transperineal MRE, and transurethral MRE. Further larger prospective study will be needed to validate it.

In the measurement of PCa, the minimum requirement of PI-RADS v2.1 is to report the largest dimension of a suspicious lesion, which is measured on mpMRI. And in the Briganti 2019 nomogram, maximum diameter of PCa is one of the variables for predicting the probability of LNM [32]. Our results showed that maximum diameter of PCa with LNM was significantly larger than that of PCa without LNM, and showed that maximum diameter of PCa 2.0 cm or more was useful for predicting LNM.

According to the guidelines, the decision to perform nodal dissection should be based on the preoperative probability of LNM [37]. The individual risk can be estimated using preoperative nomograms [32]. In our study, the risk of LNM in group 1 is eight times higher than that in group 2, based on the Briganti 2019 nomogram [32]. With the combination of PCa MRE stiffness and maximum diameter, the AUCs of the multivariate models were even higher than the AUC of the probability of predicted value calculated by the Briganti 2019 nomogram. So, the multivariate models in our study could be used as a preoperative imaging marker for predicting LNM of PCa.

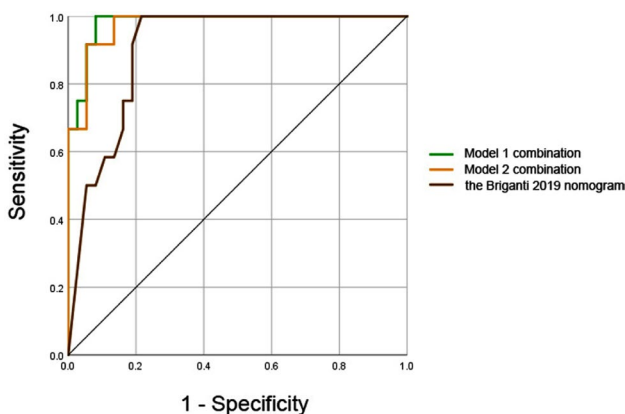


Fig. 6 Receiver operating characteristic (ROC) curves of multivariate model 1 (combination of PCa stiffness at 60 Hz and maximum diameter of PCa), model 2 (combination of PCa stiffness at 90 Hz and maximum diameter of PCa), and the probability of predicted value (calculated by the Briganti 2019 nomogram) for predicting lymph node metastasis. The areas under the curves (AUCs) of them were 0.982, 0.975, and 0.904, respectively (model 1 vs. model 2, $P = 0.383$; model 1 vs. the Briganti 2019 nomogram, $P = 0.040$; model 2 vs. the Briganti 2019 nomogram, $P = 0.060$)

Because there was collinearity between PCa MRE stiffness at 60 Hz and at 90 Hz, these two parameters couldn't be fitted in one multivariable model at the same time. So, there was no added diagnostic value by using two frequencies. Although there was no statistical difference between diagnostic efficacy of MRE at 60 Hz and 90 Hz, higher frequency provides better resolution according to MRE principle, we recommended 90 Hz for future studies.

Other MRI variables such as ADC, PCa invasiveness, and LN with restricted diffusion showed statistically significant difference between two groups in univariate analysis, but they were not independent predictors in multivariate analysis. There might be some indirect correlation between these variables and LNM of PCa.

The current study had some limitations. First, we had an inevitable selection bias because of the retrospective design. There were just 12 patients with positive LMN and only a single patient with TZ PCa with LNM. In the patient cohort only patients without LMN had PIRADS 4 scores and patients with LMN had only PIRADS 5 scores. A prospective study would be done in the future to verify the results of the current study. Second, the total number of patients was limited ($n=49$). PPV/NPV might have large errors in terms of the small number of cases. And the cases were enrolled from a single center. Further studies with larger populations in multiple centers will be needed to confirm our findings. Third, we didn't measure viscosity-related parameters, because loss modulus might not be reliable with current setup at comparable low resolution. Finally, the lesion smaller than 1 cm were excluded, the stiffness values of small lesions may be a challenge due to partial volume effects. The practical relevance of these results will also depend on the reliability and availability of MRE versus that of other emerging techniques. Under these circumstances, a higher frequency acoustic waves and focused field of view imaging have to be chosen to estimate the stiffness of small lesions accurately.

Conclusion

A combination of PCa MRE stiffness and maximum diameter can be used as a preoperative imaging marker for predicting LNM of PCa.

Supplementary Information The online version contains supplementary material available at <https://doi.org/10.1007/s00261-021-02982-4>.

Author contributions Dr. BH and Dr. YD contributed equally to the study concept and design, acquisition of data, statistical analysis, analysis and interpretation of data, drafting of the manuscript, and critical revision of the manuscript for important intellectual content.

Funding The authors state that this study has received funding by National Natural Science Foundation of China grant 91959118 (JW), Science and Technology Program of Guangzhou, China grant 201704020016 (JW), SKY Radiology Department International Medical Research Foundation of China Z-2014-07-1912-15 (JW), Clinical Research Foundation of the 3rd Affiliated Hospital of Sun Yat-sen University YHJH201901 (JW) and Key Research and Development Program of Guangdong Province 2019B020235002 (JW).

Reference

1. Cuzick J, Thorat MA, Andriole G, Brawley OW, Brown PH, Culig Z, Eeles RA, Ford LG, Hamdy FC, Holmberg L, Ilic D, Key TJ, La Vecchia C, Lilja H, Marberger M, Meyskens FL, Minasian LM, Parker C, Parnes HL, Perner S, Rittenhouse H, Schalken J, Schmid HP, Schmitz-Drager BJ, Schroder FH, Stenzl A, Tombal B, Wilt TJ, Wolk A (2014) Prevention and early detection of prostate cancer. *Lancet Oncol* 15 (11):e484–492. [https://doi.org/10.1016/S1470-2045\(14\)70211-6](https://doi.org/10.1016/S1470-2045(14)70211-6)
2. Cagiannos I, Karakiewicz P, Eastham JA, Ohori M, Rabbani F, Gerigk C, Reuter V, Graefen M, Hammerer PG, Erbersdobler A, Huland H, Kupelian P, Klein E, Quinn DI, Henshall SM, Grygiel JJ, Sutherland RL, Stricker PD, Morash CG, Scardino PT, Kattan MW (2003) A preoperative nomogram identifying decreased risk of positive pelvic lymph nodes in patients with prostate cancer. *J Urol* 170 (5):1798–1803. <https://doi.org/10.1097/01.ju.0000091805.98960.13>
3. Fossati N, Willemse PM, Van den Broeck T, van den Bergh RCN, Yuan CY, Briers E, Bellmunt J, Bolla M, Cornford P, De Santis M, MacPepple E, Henry AM, Mason MD, Matveev VB, van der Poel HG, van der Kwast TH, Rouviere O, Schoots IG, Wiegel T, Lam TB, Mottet N, Joniau S (2017) The Benefits and Harms of Different Extents of Lymph Node Dissection During Radical Prostatectomy for Prostate Cancer: A Systematic Review. *Eur Urol* 72 (1):84–109. <https://doi.org/10.1016/j.eururo.2016.12.003>
4. Crehange G, Chen CP, Hsu CC, Kased N, Coakley FV, Kurhanewicz J, Roach M, 3rd (2012) Management of prostate cancer patients with lymph node involvement: a rapidly evolving paradigm. *Cancer Treat Rev* 38 (8):956–967. <https://doi.org/10.1016/j.ctrv.2012.05.005>
5. Hovels AM, Heesakkers RA, Adang EM, Jager GJ, Strum S, Hoogeveen YL, Severens JL, Barentsz JO (2008) The diagnostic accuracy of CT and MRI in the staging of pelvic lymph nodes in patients with prostate cancer: a meta-analysis. *Clin Radiol* 63 (4):387–395. <https://doi.org/10.1016/j.crad.2007.05.022>
6. von Below C, Daouacher G, Wassberg C, Grzegorek R, Gestblom C, Sorensen J, Ahlstrom H, Walden M (2016) Validation of 3 T MRI including diffusion-weighted imaging for nodal staging of newly diagnosed intermediate- and high-risk prostate cancer. *Clin Radiol* 71 (4):328–334. <https://doi.org/10.1016/j.crad.2015.12.001>
7. Czarniecki M, Caglic I, Grist JT, Gill AB, Lorenc K, Slough RA, Priest AN, Barrett T (2018) Role of PROPELLER-DWI of the prostate in reducing distortion and artefact from total hip replacement metalwork. *Eur J Radiol* 102:213–219. <https://doi.org/10.1016/j.ejrad.2018.03.021>
8. Winter A, Woenkhaus J, Wawroschek F (2014) A novel method for intraoperative sentinel lymph node detection in prostate cancer patients using superparamagnetic iron oxide nanoparticles and a handheld magnetometer: the initial clinical experience. *Ann Surg Oncol* 21 (13):4390–4396. <https://doi.org/10.1245/s10434-014-4024-8>

9. Chang CH, Wu HC, Tsai JJ, Shen YY, Changlai SP, Kao A (2003) Detecting metastatic pelvic lymph nodes by 18F-2-deoxyglucose positron emission tomography in patients with prostate-specific antigen relapse after treatment for localized prostate cancer. *Urol Int* 70 (4):311–315. <https://doi.org/10.1159/000070141>
10. Muteganya R, Goldman S, Aoun F, Roumequere T, Albisinni S (2018) Current Imaging Techniques for Lymph Node Staging in Prostate Cancer: A Review. *Front Surg* 5:74. <https://doi.org/10.3389/fsurg.2018.00074>
11. Phipps S, Yang TH, Habib FK, Reuben RL, McNeill SA (2005) Measurement of tissue mechanical characteristics to distinguish between benign and malignant prostatic disease. *Urology* 66 (2):447–450. <https://doi.org/10.1016/j.urology.2005.03.017>
12. Yuan S, Magarik M, Lex AM, Fleischer AC (2016) Clinical applications of sonoelastography. *Expert Rev Med Devices* 13 (12):1107–1117. <https://doi.org/10.1080/17434440.2016.1257938>
13. Koh J, Jung DC, Oh YT, Yoo MG, Noh S, Han KH, Rha KH, Choi YD, Hong SJ (2015) Additional Targeted Biopsy in Clinically Suspected Prostate Cancer: Prospective Randomized Comparison between Contrast-Enhanced Ultrasound and Sonoelastography Guidance. *Ultrasound Med Biol* 41 (11):2836–2841. <https://doi.org/10.1016/j.ultrasmedbio.2015.06.024>
14. Woo S, Suh CH, Kim SY, Cho JY, Kim SH (2017) Shear-Wave Elastography for Detection of Prostate Cancer: A Systematic Review and Diagnostic Meta-Analysis. *AJR Am J Roentgenol* 209 (4):806–814. <https://doi.org/10.2214/AJR.17.18056>
15. Sarvazyan A, Hall TJ, Urban MW, Fatemi M, Aglyamov SR, Garra BS (2011) An Overview of Elastography - an Emerging Branch of Medical Imaging. *Curr Med Imaging Rev* 7 (4):255–282
16. Venkatesh SK, Ehman RL (2015) Magnetic resonance elastography of abdomen. *Abdom Imaging* 40 (4):745–759. <https://doi.org/10.1007/s00261-014-0315-6>
17. Wang J, Deng Y, Jondal D, Woodrum DM, Shi Y, Yin M, Venkatesh SK (2018) New and Emerging Applications of Magnetic Resonance Elastography of Other Abdominal Organs. *Top Magn Reson Imaging* 27 (5):335–352. <https://doi.org/10.1097/RMR.0000000000000182>
18. Loomba R, Wolfson T, Ang B, Hooker J, Behling C, Peterson M, Valasek M, Lin G, Brenner D, Gamst A, Ehman R, Sirlin C (2014) Magnetic resonance elastography predicts advanced fibrosis in patients with nonalcoholic fatty liver disease: a prospective study. *Hepatology* 60 (6):1920–1928. <https://doi.org/10.1002/hep.27362>
19. Yasar TK, Wagner M, Bane O, Besa C, Babb JS, Kannengieser S, Fung M, Ehman RL, Taouli B (2016) Interplatform reproducibility of liver and spleen stiffness measured with MR elastography. *J Magn Reson Imaging* 43 (5):1064–1072. <https://doi.org/10.1002/jmri.25077>
20. Kirpalani A, Hashim E, Leung G, Kim JK, Krizova A, Jothy S, Deeb M, Jiang NN, Glick L, Mnatzakanian G, Yuen DA (2017) Magnetic Resonance Elastography to Assess Fibrosis in Kidney Allografts. *Clin J Am Soc Nephrol* 12 (10):1671–1679. <https://doi.org/10.2215/CJN.01830217>
21. Kolipaka A, Schroeder S, Mo X, Shah Z, Hart PA, Conwell DL (2017) Magnetic resonance elastography of the pancreas: Measurement reproducibility and relationship with age. *Magn Reson Imaging* 42:1–7. <https://doi.org/10.1016/j.mri.2017.04.015>
22. Thormer G, Reiss-Zimmermann M, Otto J, Hoffmann KT, Moche M, Garnov N, Kahn T, Busse H (2013) Novel technique for MR elastography of the prostate using a modified standard endorectal coil as actuator. *J Magn Reson Imaging* 37 (6):1480–1485. <https://doi.org/10.1002/jmri.23850>
23. Sahebjavaher RS, Baghani A, Honarvar M, Sinkus R, Salcudean SE (2013) Transperineal prostate MR elastography: initial in vivo results. *Magn Reson Med* 69 (2):411–420. <https://doi.org/10.1002/mrm.24268>
24. Chopra R, Arani A, Huang Y, Musquera M, Wachsmuth J, Bronskill M, Plewes D (2009) In vivo MR elastography of the prostate gland using a transurethral actuator. *Magn Reson Med* 62 (3):665–671. <https://doi.org/10.1002/mrm.22038>
25. Sahebjavaher RS, Nir G, Gagnon LO, Ischia J, Jones EC, Chang SD, Yung A, Honarvar M, Fazli L, Goldenberg SL, Rohling R, Sinkus R, Kozlowski P, Salcudean SE (2015) MR elastography and diffusion-weighted imaging of ex vivo prostate cancer: quantitative comparison to histopathology. *NMR Biomed* 28 (1):89–100. <https://doi.org/10.1002/nbm.3203>
26. Li S, Chen M, Wang W, Zhao W, Wang J, Zhao X, Zhou C (2011) A feasibility study of MR elastography in the diagnosis of prostate cancer at 3.0T. *Acta Radiol* 52 (3):354–358. <https://doi.org/10.1258/ar.2010.100276>
27. Dittmann F, Reiter R, Guo J, Haas M, Asbach P, Fischer T, Braun J, Sack I (2018) Tomoelastography of the prostate using multi-frequency MR elastography and externally placed pressurized-air drivers. *Magn Reson Med* 79 (3):1325–1333. <https://doi.org/10.1002/mrm.26769>
28. Manduca A, Oliphant TE, Dresner MA, Mahowald JL, Kruse SA, Amromin E, Felmlee JP, Greenleaf JF, Ehman RL (2001) Magnetic resonance elastography: non-invasive mapping of tissue elasticity. *Med Image Anal* 5 (4):237–254. [https://doi.org/10.1016/S1361-8415\(00\)00039-6](https://doi.org/10.1016/S1361-8415(00)00039-6)
29. Yin M, Rouviere O, Glaser KJ, Ehman RL (2008) Diffraction-biased shear wave fields generated with longitudinal magnetic resonance elastography drivers. *Magn Reson Imaging* 26 (6):770–780. <https://doi.org/10.1016/j.mri.2008.01.019>
30. Arunachalam SP, Rossman PJ, Arani A, Lake DS, Glaser KJ, Trzasko JD, Manduca A, McGee KP, Ehman RL, Araoz PA (2017) Quantitative 3D magnetic resonance elastography: Comparison with dynamic mechanical analysis. *Magn Reson Med* 77 (3):1184–1192. <https://doi.org/10.1002/mrm.26207>
31. Turkbey B, Rosenkrantz AB, Haider MA, Padhani AR, Villeirs G, Macura KJ, Tempny CM, Choyke PL, Cornud F, Margolis DJ, Thoeny HC, Verma S, Barentsz J, Weinreb JC (2019) Prostate Imaging Reporting and Data System Version 2.1: 2019 Update of Prostate Imaging Reporting and Data System Version 2. *Eur Urol*. <https://doi.org/10.1016/j.eururo.2019.02.033>
32. Gandaglia G, Ploussard G, Valerio M, Mattei A, Fiori C, Fossati N, Stabile A, Beauval JB, Malavaud B, Roumiguie M, Robesti D, Dell'Oglio P, Moschini M, Zamboni S, Rakauskas A, De Cobelli F, Porpiglia F, Montorsi F, Briganti A (2019) A Novel Nomogram to Identify Candidates for Extended Pelvic Lymph Node Dissection Among Patients with Clinically Localized Prostate Cancer Diagnosed with Magnetic Resonance Imaging-targeted and Systematic Biopsies. *Eur Urol* 75 (3):506–514. <https://doi.org/10.1016/j.eururo.2018.10.012>
33. Asbach P, Ro SR, Aldoj N, Snellings J, Reiter R, Lenk J, Kohlitz T, Haas M, Guo J, Hamm B, Braun J, Sack I (2020) In Vivo Quantification of Water Diffusion, Stiffness, and Tissue Fluidity in Benign Prostatic Hyperplasia and Prostate Cancer. *Invest Radiol* 55 (8):524–530. <https://doi.org/10.1097/RLI.0000000000000685>
34. Reiter R, Majumdar S, Kearney S, Kajdacsy-Balla A, Macias V, Crivellaro S, Caldwell B, Abern M, Royston TJ, Klatt D (2020) Prostate cancer assessment using MR elastography of fresh prostatectomy specimens at 9.4 T. *Magn Reson Med* 84 (1):396–404. <https://doi.org/10.1002/mrm.28127>
35. Pepin KM, Ehman RL, McGee KP (2015) Magnetic resonance elastography (MRE) in cancer: Technique, analysis, and applications. *Prog Nucl Magn Reson Spectrosc* 90–91:32–48. <https://doi.org/10.1016/j.pnmrs.2015.06.001>
36. Chen J, Alexander JS, Orr AW (2012) Integrins and their extracellular matrix ligands in lymphangiogenesis and lymph node metastasis. *Int J Cell Biol* 2012:853703. <https://doi.org/10.1155/2012/853703>

37. Mottet N, Bellmunt J, Bolla M, Briers E, Cumberbatch MG, De Santis M, Fossati N, Gross T, Henry AM, Joniau S, Lam TB, Mason MD, Matveev VB, Moldovan PC, van den Bergh RCN, Van den Broeck T, van der Poel HG, van der Kwast TH, Rouviere O, Schoots IG, Wiegel T, Cornford P (2017) EAU-ESTRO-SIOG Guidelines on Prostate Cancer. Part 1: Screening, Diagnosis, and

Local Treatment with Curative Intent. *Eur Urol* 71 (4):618-629. <https://doi.org/10.1016/j.eururo.2016.08.003>

Publisher's Note Springer Nature remains neutral with regard to jurisdictional claims in published maps and institutional affiliations.